-RESEARCH PAPER-

International Journal of Mining and Geo-Engineering

IJMGE

IJMGE 60-3 (2026) 347-356

DOI: 10.22059/IJMGE.2026.408790.595349

Euler deconvolution of a localized secondary fault of toru segment: the Batu Jomba landslide-prone road corridor

Nadiyah Az Zuhriyyah [a, *], Lailatul Husna Lubis [a], Rahmat Nawi Siregar [b] and Russell Ong [a]

[a] *Department of Physics, Universitas Islam Negeri Sumatera Utara, Indonesia.*

[b] *Department of Physics, Institut Teknologi Sumatera, Indonesia.*

Article History:

Received: 26 December 2025.

Revised: 19 February 2026.

Accepted: 22 September 2026.

ABSTRACT

Landslide mitigation in active tectonic regions is a critical component of geo-environmental risk management, particularly in areas with steep topography near active fault zones. This study applies the Euler deconvolution formula on gravity data to delineate the presence of a localized secondary fault associated with the Toru Segment (a part of the Sumatran Fault Zone), within the landslide-prone road corridor in Batu Jomba. Previous studies in this area have primarily focused on fault slip rates and shallow-depth fault mapping, therefore, the detection of secondary fault activity intersecting the Toru Segment has not been explored. To address this gap, high-resolution gravity anomaly data from the GGMplus model (~200 m resolution) were processed using geophysical inversion to image subsurface density variations and Euler deconvolution formula was applied to estimate the depth of these two areas. The Batu Jomba area is characterized by a low Bouguer density of 2.0454 g/cm³, consistent with the Sihapas Formation dominated by weak sandstone lithology. Field observations corroborate the presence of sandstone boulders within the landslide body, indicating low material strength. Euler deconvolution results reveal the absence of direct structural expression beneath the Batu Jomba. However, clustered depth solutions in areas surrounding Batu Jomba delineate the presence of localized secondary fault at depths of 193-530 m, nearby the main Toru Segment. Regional Euler depth patterns indicate tectonic activity at depths of 193-590 m in part of the Toru Segment and 193-1,082 m in the Angkola Segment. The shallower depth extent of the Toru Segment and Batu Jomba area when compared to the Angkola Segment supports the interpretation of localized crustal thinning in the Toru Segment region at shallow depths. These findings indicate that the Batu Jomba landslide-prone road corridor is controlled primarily by weak lithology and the nearby presence of secondary fault rather than the main Toru Segment. The results highlight the effectiveness of gravimetric methods, particularly Euler deconvolution in characterizing fault activity and geo-hazard assessment, offering practical implications for engineering planning and disaster-risk reduction.

Keywords: *Batu Jomba, Euler deconvolution, Secondary fault, Toru segment.*

1. Introduction

Landslides occurring within active fault zones represent a major geo-environmental hazard in many tectonically complex regions worldwide. Recent studies, such as the investigation of the Nanpeng River fault zone in China [1] have shown that fault activity can directly influence slope deformation and strongly affect the spatial distribution of unstable slopes. Understanding the behaviour of subsurface structures is therefore essential, as these structures including stratigraphic layers, geological formations, faults, folds, aquifers, and mineral or hydrocarbon deposits. Depending on geological settings, these subsurface elements may be homogeneous with uniform hydraulic conductivity or highly heterogeneous, exhibiting variations in conductivity across locations [2, 3]. Accurate information of these structures is crucial for guiding engineering decisions and development planning, particularly in landslide-prone areas such as Batu Jomba.

The Batu Jomba region, located at the North Sumatran crossroads, has repeatedly experienced ground deformation and landslides since 1997. The area is situated on the left side near the Toru Segment of the Sumatran Fault Zone. A major landslide in Aek Latong in 2002 resulted in the relocation of residents [4]. Previous geophysical investigations, including the Schlumberger geoelectrical surveys, have indicated the presence of weak zones and rock fractures that trigger soil deformation around Batu Jomba [5]. In addition, Ground Penetrating Radar (GPR) analysis has identified fault traces cutting through soil and rock layers beneath the road, as well as deformation within breccia and tuffaceous sand layers. These fractured units facilitate displacement without significant energy accumulation, suggesting that the Toru Fault Segment may be deforming in an aseismic manner, without generating large earthquakes.

The Toru Segment itself plays a central role in regional tectonic activity, exhibiting a slip rate of 9,3 mm/year with an uncertainty of ±1,8 mm/year [6]. Observations by the National Road Management Agency I indicate that ground displacement in Batu Jomba continues at approximately 1–5 cm every two weeks [7]. This segment forms part of the Sumatran Fault Zone, located between latitudes 1,2° N and 2,0° N and is characterized as a strike-slip fault with a length of 95 km. Historically, the Toru Segment has generated significant earthquakes in 1984 (Ms 6.4) and 1987 (Ms 6.6). The segment also connects to deeper seismicity within the Benioff Zone at depths of 125-155 km [8]. Despite

* Corresponding author. *E-mail address:* ndyzy14@gmail.com (N.A Zuhriyyah).

its active behaviour, the extent to which deeper fault structures influence the recurrent landslide in Batu Jomba remain unclear. Geophysical method, particularly gravity surveying is widely used to detect subsurface density variations and has long been applied in hydrocarbon exploration [9]. When applied to fault zones, this gravity anomalies offer an effective means of mapping fault geometry due to density contrasts across fractured and unfractured rock masses [10]. A key advancement in gravity interpretation is Euler deconvolution, which estimates the depth, position, and geometric nature of anomaly sources by applying Euler's differential equation to gravity data [11]. This approach has been successfully implemented to find the depth of Lembang Fault [12] and tin-bearing zones in Okeso, Nigeria [13].

Recent applications show that Euler deconvolution is also capable of resolving secondary and deep-seated fault systems. Studies in Victoria, Australia, have used depth-solution clustering from aeromagnetic and global magnetic datasets to map both major and subsidiary faults from shallow to deep crustal levels [14]. Similar approaches in the Adamaoua Plateau (Cameroon) confirmed known fault structures while revealing previously unmapped fault systems at depths >20 km [15]. In northeast India, the application of 3D Euler deconvolution has also successfully delineated thrust-faults, validating existing boundaries while identifying additional secondary faults within the tectonically complex Himalayan–Indo-Burman convergence zone [16].

These findings demonstrate the method's strength in identifying hidden structural controls in tectonically complex regions. Despite extensive research in Batu Jomba and the Toru Segment, previous studies have predominantly focused on fault slip rates and shallow structural mapping, leaving the possibility of deeper or secondary fault activity largely unexplored. To address this gap, the present study applies high-resolution gravity anomaly data from the GGMplus model (~200 m resolution) combined with Euler deconvolution to determine whether the subsurface depth characteristics beneath Batu Jomba correspond to the geometry of the Toru Segment or indicate the presence of a previously unidentified secondary fault.

2. Geological setting

2.1. Regional geology

Batu Jomba is located in Luat Lombang Village, Sipirok District, South Tapanuli Regency, precisely at coordinates 1°37'40" North Latitude (N) and 99°12'10" East Longitude (E). This area comprises a newly constructed national road segment that is highly susceptible to ground deformation, particularly landslides. Previously, this road was relocated from the route in Aek Latong Lama Village, which had similar conditions. In the Batak language, *Batu* means "stone" and "kilometer," while *Jomba* means "leaning," "tilted," or "sliding forward".

This name reflects the geographical characteristics of the area where the terrain is steep and unstable. Situated within the influence of the Toru Segment, Batu Jomba is highly vulnerable to tectonic activity and slope failures. Continuous displacement and repeated landslides have made this corridor a critical zone for geological and geotechnical investigation, particularly for understanding fault-controlled deformation and its implication for infrastructure stability.

Figure 1 presents a 3D perspective map, illustrating the regional setting, including the Batu Jomba landslide-prone road corridor (upper-left inset) and major geological structures such as the Sarulla Graben and the stratovolcanoes Sibualbuali and Lubukraya. Several nearby towns such as Sipirok, Batang Toru, and Padang Sidempuan—are also indicated to provide spatial context.

The two inset graphs provide supporting seismic information; (a) A Vp/Vs cross-plot showing two distinct clusters where the higher Vp/Vs values (pink region) represent fluid-bearing and fractured sediments within the graben. (b) The spatial distribution of these anomalous seismic zones along the Sarulla Graben, suggesting that fluids migrate along fault conduits and may transport heat from deeper crustal levels to the surface [17]. Together, these datasets highlight the active tectonic and hydrogeological processes that contribute to slope instability in the Batu Jomba region.

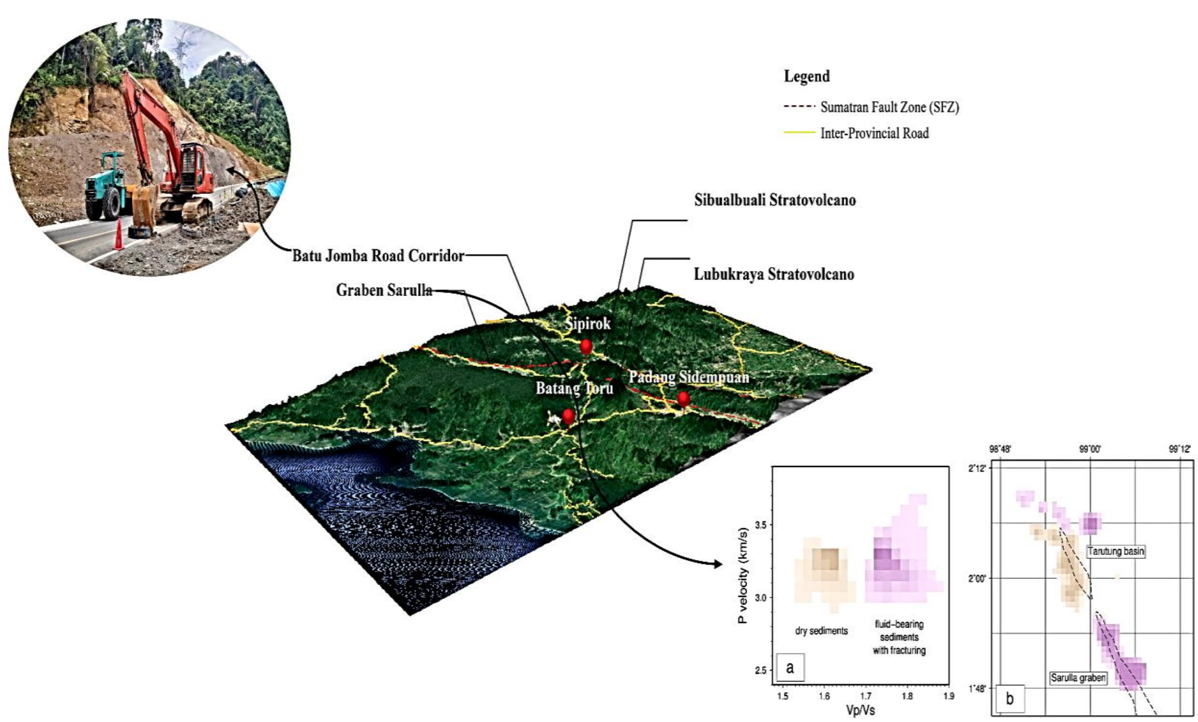

Figure 1. Geological and tectonic setting of the Batu Jomba Road Corridor along the Sumatran Fault Zone (SFZ). The map shows the inter-provincial road and Sarulla Graben, accompanied by (a) Vp/Vs clustering that differentiates dry sediments from fluid-bearing fractured sediments, and (b) the spatial distribution of these seismic anomalies within the graben [17].

Figure 2 illustrates the complex tectonic and topographic setting surrounding Batu Jomba. Figure 2a presents a Digital Elevation Model (DEM) with 30 meters resolution derived from SRTM data, displaying elevation variations ranging from -43 to 4,485 meters above sea level. The color-coded legend indicates elevation zones: gray for the lowest elevations (-43 to 862.6 m), yellow-green for moderate elevations (862.6 to 2,673.8 m), blue for higher elevations (2,673.8 to 3,579.4 m), and red for the highest peaks (3,579.4 to 4,485 m). The map clearly delineates the Batu Jomba Road corridor (outlined in red) situated in proximity to major tectonic features, including the Toru Segment of the Sumatran Fault Zone (shown by red lines) and the Sarulla Graben to the northwest. The southern region is dominated by the Sibualbuali and Lubukraya stratovolcanoes, visible as prominent red peaks indicating high elevations exceeding 3,500 meters. The topographic variations across the landscape reflect active deformation associated with these major geological structures.

The Toru Segment forms part of the dextral strike-slip Sumatran Fault and extends from Central Tapanuli Regency to South Tapanuli Regency, playing a significant role in accommodating crustal deformation in North Sumatra. Geodetic and geological studies indicate that the Toru Segment exhibits creeping behavior along parts of its fault plane, where the fault slips aseismically due to low frictional resistance. Fault creep allows gradual displacement without the build-up of significant elastic strain, resulting in limited large-magnitude earthquakes.

This is consistent with the historical seismic record which shows that the Toru Segment has not generated major events (M≥7), with its most notable earthquake being the 1987 Ms 6.6 event. Modern estimates place the slip rate of the Toru Segment at approximately 9–10 mm/yr, with an uncertainty of ±1.8 mm/yr [6] confirming its status as an active but predominantly creeping structure. This creeping behavior has important implications for slope instability in Batu Jomba, where continuous slow deformation likely contributes to repeated landslide occurrences along the road corridor.

2.2. Local geology

Batu Jomba, the research area, is of Miocene age, formed approximately 23–5,3 million years ago. Marine sandstones and limestones of Miocene age occur along the margins of the back-arc basin of Sumatra. The Silangkitang well, drilled within the Sarulla Basin, encountered conglomerates rich in volcanic clasts, overlain by more than 2 km of interbedded tuff and lacustrine siltstone. Radiometric dating of volcanic rocks in the Sarulla area indicates that volcanic activity commenced around 1,8 million years ago. Mount Sibualbuali is a stratovolcano composed of successive andesite lava flows and breccias, intercalated with several tuff layers, with ages ranging from 0,7 to 0,3 million years ago. The distribution and basal elevation of the older tuffs of Mount Sibualbuali indicate that these tuffs have migrated northward from the volcano [18].

The geological time scale shown in Figure 3 (left) illustrates the chronological system used to describe Earth's history based on the age of rocks, fossils, and geological events from 4,6 billion years ago to the present. For the research area, the digitized geological time scale indicates the Middle Miocene period, which occurred approximately 15,97 to 11,63 million years ago.

This period was characterized by a warmer climate and the emergence of many new species. The migration of volcanism in northwest Sumatra during the Middle Miocene was influenced by the far-field effects of the Eurasian Plate collision, which caused the oblique subduction system in Sumatra to evolve into a plate boundary with dextral strike-slip motion [19]. The magmatic arc shown in Figure 3 (right) represents the zone where magma is generated beneath the earth's crust as a result of partial melting of the mantle caused by plate subduction.

In contrast, the volcanic arc refers to the chain of volcanoes that form at the surface due to volcanic activity driven by the magma produced in the magmatic arc. In the research area, the tectonic setting corresponds to a Subduction Continent-Oceanic type (Back-Arc), which is the region located behind the volcanic arc formed when the oceanic plate subducts beneath the continental plate.

This process often results in the development of a back-arc basin that serves as a site for sediment accumulation. The back-arc is characterized by decreasing temperature and pressure, as well as the generation of new magma that can trigger volcanic activity. Mantle upwelling in the Sumatran back-arc basin supplies magma and generates a heat flow exceeding 100 mW/m², making it one of the highest heat flow regions in the world. This thermal anomaly indicates significant potential for geothermal energy utilization in the Sumatran back-arc basin [20].

The geological map of the Batu Jomba area shown in Figure 4 reveals the region's topographic and lithological characteristics.

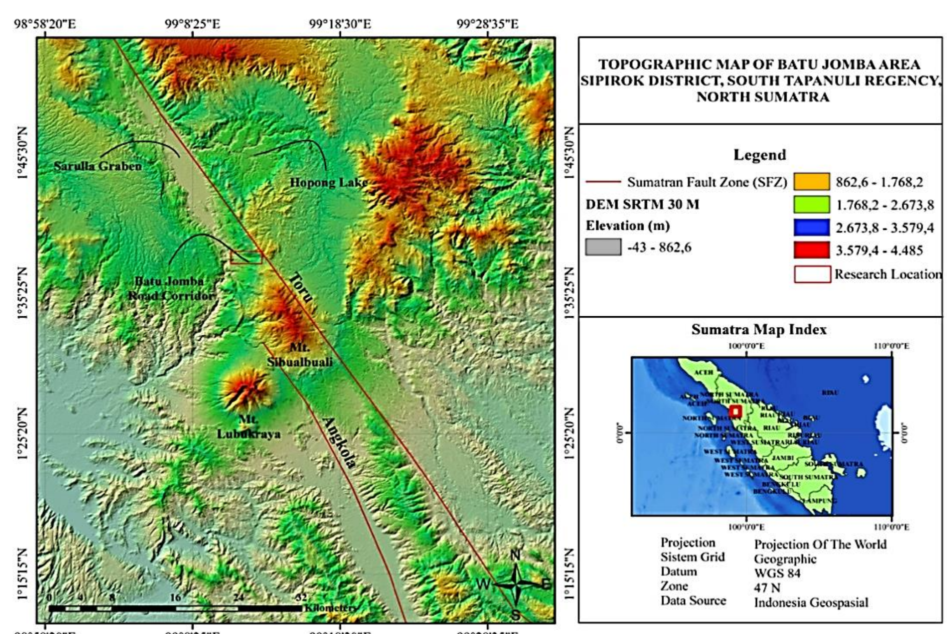

Figure 2. Topographic map of the Batu Jomba area: (a) Digital elevation map (DEM) showing the Sumatra Fault Zone (SFZ), the Sarulla Graben, stratovolcanoes (Mt. Sibualbuali and Mt. Lubukraya) and the Batu Jomba Road corridor as the main research location (left side), and (b) Sumatra map index showing the regional context of the study within North Sumatra (right side).

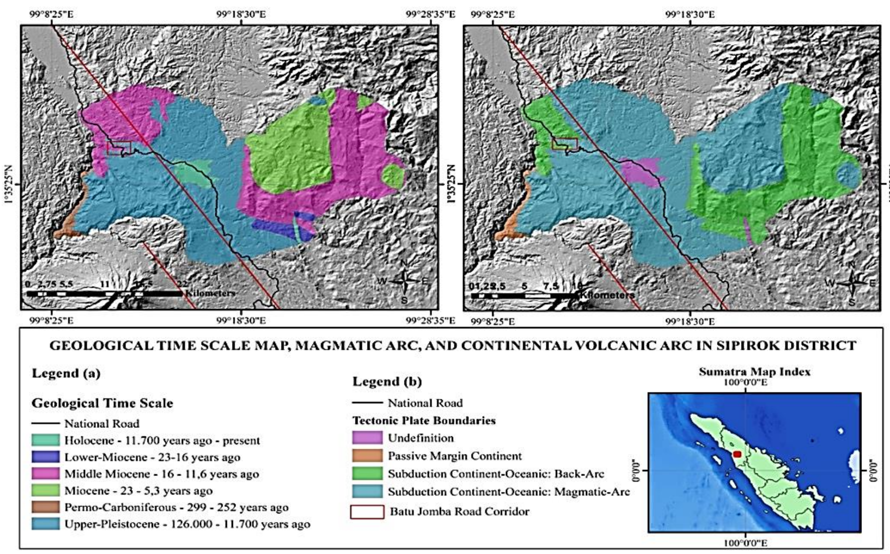

Figure 3. Geological framework of the Batu Jomba Road corridor in Sipirok District highlighting middle miocene geological time scale map (left side) and subduction continent-oceanic boundaries in relation to the Sumatra Fault Zone (SFZ) (right side).

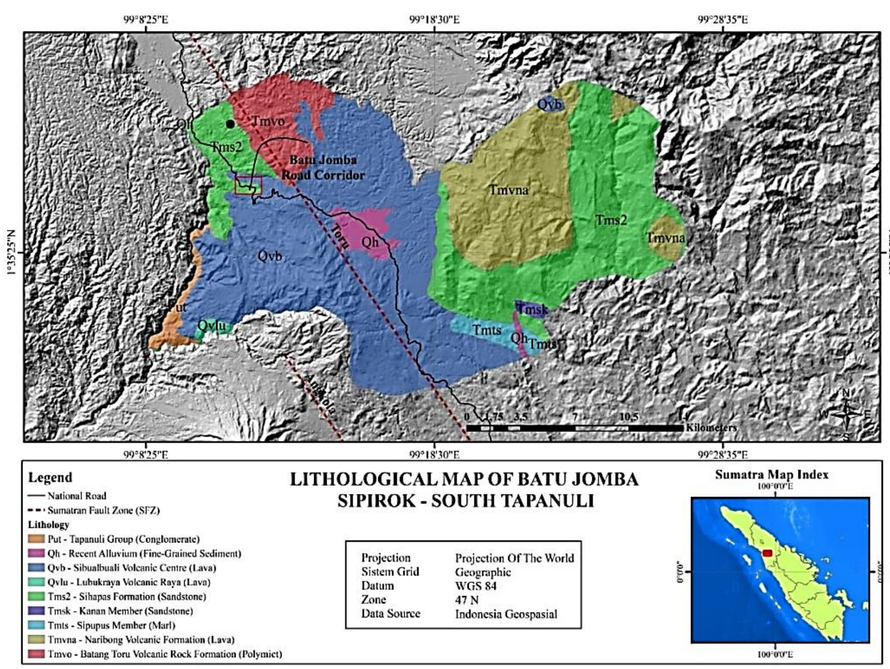

Figure 4. Lithological map of the Batu Jomba area by Sihapas Formation, characterized by sandstone lithology.

Figure 4 presents the detailed lithological distribution, showing that the region is dominated by several rock formations, with the Sihapas Formation (Tms2) being the most prominent. This formation is part of the stratigraphy of the Central Sumatra Basin, dated to the Early to Middle Miocene. It is composed of quartz sandstone, carbonaceous shale, siltstone, and conglomerate, and serves as a major hydrocarbon reservoir [21]. The upper part of the Sihapas Formation consists of fluvial–deltaic sandstones derived from the Malaysian Shield, deposited through a braided river system and a deltaic river system that prograde into the sea [22].

3. Materials and methods

3.1. Gravity method

The gravity method is based on variations in the density of subsurface materials. As a passive geophysical method, measurements are carried out without injecting any signal into the Earth. This method is often applied as a preliminary survey in exploration, particularly to identify subsurface geological structures [23]. Earth's gravity is influenced not only by elevation and geographic position but also by subsurface geological factors. Variations in rock density, the presence of geological structures such as faults, folds, joints, fractures, material distribution, and even magma intrusions can generate gravity anomalies in a given region. A study of barite deposits in the Red River Hills of Sudan using multispectral and hyperspectral satellite data, integrated with field investigations, revealed that barite mineralization zones are associated with high gravity anomalies in the range of 0,0007–0,0009 mGal [24]

In this study, gravity data were obtained from the GGMPlus dataset, a high-resolution global gravity model available at https://ddfe.curtin.edu.au/models/GGMplus/ with a spatial resolution of ~200 meters. The dataset incorporates a combined solution from three satellite missions, namely GOCE/GRACE, EGM2008, and topographic gravity data [24]. The accuracy of GGMPlus gravity data compared to field measurements has been reported to reach 1,45% [25].

The GGMPlus dataset downloaded using the coordinate tile code "N00E95" is initially in raw format and requires extraction to obtain usable data for subsequent gravity corrections. The extraction process was carried out using MATLAB by inputting the coordinates of the study area and applying a script containing an interpolation function. The MATLAB script used for the gravity data extraction is available at https://github.com/yayacomel14/Matlab-Script-for-Gravity-Data-Extraction.

A cubic interpolation function which employs a third-order polynomial, was used to estimate values between grid points. In interpolation, the higher the number of data points, the higher the polynomial order that can be applied. Cubic interpolation is generally preferred because it produces a smoother and more accurate approximation of the data [26].

3.2. Depth estimation with euler deconvolution

Interpretation of geophysical data, including gravity data, is often a time-consuming process, particularly when dealing with large datasets. To address this, semi-automatic interpretation techniques are employed as an initial step to provide estimates of key parameters, such as the location and depth of anomalous sources. The Euler homogeneity function theorem plays an important role in both physics and mathematics, stating that for a homogeneous function of degree *N*, a specific relationship exists between the function and its partial derivatives [27]. By utilizing the horizontal and vertical derivatives of the gravity potential field, Euler's equation can be applied to reliably estimate the depth of subsurface sources [28]. Beyond depth estimation, the Euler system of equations is also useful for delineating anomaly boundaries and discontinuity depths. The fundamental mathematical concept of Euler's homogeneity equation for the gravity field can be expressed as follows:

$$(x - x_0)\frac{\partial Pg}{\partial x} + (y - y_0)\frac{\partial Pg}{\partial y} + (z - z_0)\frac{\partial Pg}{\partial z} = Ng(Bg - Pg) \quad (1)$$

Equation (1) briefly describes the parameter of the gravity data observed at the point (x, y, z) where $\frac{\partial Pg}{\partial x}, \frac{\partial Pg}{\partial y}, \frac{\partial Pg}{\partial z}$ represent the directional derivatives of the gravity potential field, which can ve computed using methods such as convolution in the Fourier domain. The variables x_0, y_0, z_0 denote the coordinates of the gravity anomaly source, while x, y, z correspond to the coordinates of the observation point. The parameter z_0 indicates the depth of the gravity potential field source. Furthermore, Bg represents the regional or background gravity field data, P_g is the gravity potential value at the observation point (x, y, z) and N denotes the degree of homogeneity of the potential field.

4. Data interpretation

4.1. Average density

After obtaining the Free-Air Anomaly and X-Parasnis values, the two columns of data were plotted into a graph. Based on the graph, a fairly strong positive linear correlation is observed, with a regression equation of y=2,0454x+4.3803 and a coefficient of determination of R^2=0,8348. This coefficient indicates that approximately 83,48% of the variation in the average density accuracy within the study area is explained by the model, yielding an average density of 2,0454 g/cm³. The R^2 value is used to measure how well the independent variable (x) explains the variation of the dependent variable (y). The higher the R^2 value, the better the model predicts and explains the relationship between x and y [27].

According to the rock density table [28] this density value corresponds to sedimentary rocks such as highly porous sandstone, compacted clay, or fine-grained sedimentary rocks like shale or siltstone that have not undergone significant compaction or cementation. This indicates that the study area potentially contains thick sedimentary layers associated with structural basins or depressions. Acoustic impedance inversion and multi-attribute seismic studies on sandstone in the Bonaparte Basin also reveal sandstone lithologies with similar densities to those found in Batu Jomba, ranging from 2,1 to 2,3 g/cm³ which indicate hydrocarbon gas accumulation zones [29].

4.2. Bouguer anomaly

The complete Bouguer anomaly (CBA) results present gravity anomaly data that have been fully corrected, including topographic corrections, thereby providing a more accurate representation of subsurface rock density variations. The CBA values in the study area range from −1141,116 mGal to −38,153 mGal. The map displays smooth color gradients and contours that reflect distinct differences in the distribution of geological mass. Blue-to-green gradients represent low gravity anomalies, which dominate the areas of Mount Lubukraya, Mount Sibual-buali, Aek Nabara, and Sipirok. Meanwhile, yellow-to-pink gradients represent high gravity anomalies, covering Simangumban, Batu Jomba, Batang Toru, Padang Sidempuan, and Pargaroetan. The CBA value at Batu Jomba is −370,207 mGal.

According to [30], negative Bouguer anomaly values are typically observed in sedimentary basins and indicate subsurface areas with low density. Study [30] reported that low Bouguer anomaly values, reaching −96 mGal, with relatively higher anomalies above them in the Sumatra Basin, indicate the presence of low-density mantle bodies intruded by higher-density igneous material. This pattern reflects crustal thinning beneath North Sumatra, caused by regional extensional stress from the mantle at depths of approximately 20 km.

The regional anomaly values in this area range from −1109,4 mGal to −50,207 mGal. The map reveals smooth and widely distributed contour patterns, suggesting gradual changes in rock mass density at deeper levels around ~875,1135 meters. Low anomalies at this depth are distributed across Mount Lubukraya, Mount Sibual-buali, Sipirok, and Aek Nabara. In contrast, high anomalies occur in Simangumban, Batu Jomba, Batang Toru, Padang Sidempuan, and Pargaroetan. These high- and low-anomaly distributions help identify large structural zones that may influence basin formation and regional geological systems.

Meanwhile, the residual anomaly map provides more detailed information on shallow geological structures at depths of ~278.7838 meters. Residual anomaly values in the study area range from −130,112 mGal to 118,126 mGal. The contour patterns appear denser, more complex, and exhibit tightly spaced color variations, reflecting subsurface density changes at shallow depths. Residual anomalies were obtained by narrowing the spectral filter range of the regional anomalies. Study [31] on gravity anomalies at Mount Sibual-buali reported residual anomaly values ranging from −0,1 mGal to 0,15 mGal.

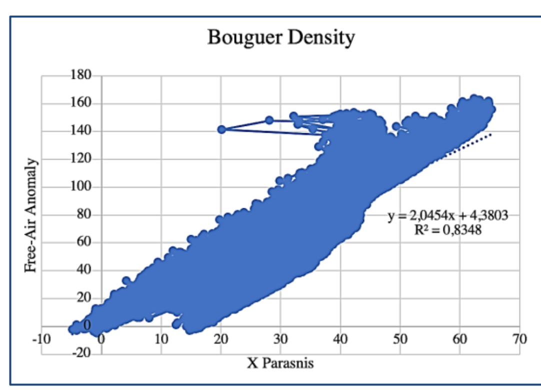

Figure 5. Average Bouguer density determined by the Parasnis method, with a regression equation y = 2,0454x + 4,3803 (average density = 2,0454 g/cm3; R2 = 0,8348 indicating model reliability).

4.3. Spectral analysis

The analyzed Bouguer anomaly consists of a combination of regional and residual anomalies. Identifying the depths of these two types of anomalies is an essential step in the interpretation process to determine the location and depth of the target. This process utilizes Fourier transformation to convert the data from the spatial domain into the frequency or wavenumber domain, thereby enabling a more detailed spectral analysis. Equation (2) describes the exponential attenuation of gravity anomaly amplitudes in the frequency domain as a function of source depth. After applying the Fourier transform to the gravity anomaly data, the logarithm of the radially averaged power spectrum is linearly related to the wavenumber. If spatial frequency f is used, the relationship can be expressed as:

$$InA(f) = InA_0 - 4\pi z f \quad (2)$$

where $A(f)$ denotes the spectral amplitude, z represents the depth to the anomaly source, and f is the spatial frequency (m^{-1}). This formulation follows the classical spectral analysis approach for potential field data [32]. In practical applications, depth estimation is performed by plotting the logarithm of the radially averaged power spectrum against the wavenumber. Under the assumption of randomly distributed sources at a common depth, the logarithmic spectrum exhibits a linear segment. The slope of this linear trend is directly proportional to the source depth. Therefore, the depth to the anomaly source can be estimated through linear regression applied to the selected portion of the log-spectrum. This method provides a robust and widely accepted approach for determining average source depths in gravity and magnetic data interpretation.

Based on the spectral analysis of the potential field data presented in Figure 7, it can be observed that the spectral components are divided into three main zones: regional, local, and noise. The regional zone corresponds to the low-wavenumber (low-frequency) portion of the spectrum and reflects large-scale gravity anomalies related to deeper geological structures, such as the crust–mantle boundary. The local zone encompasses intermediate wavenumbers and represents shallower geological structures such as faults, intrusions, or sedimentary rocks. Meanwhile, the noise zone appears at high wavenumbers (high frequencies) and mainly reflects disturbances from surface effects.

To determine the spectral analysis equation, linear regression (y=mx+c) was applied to each zone. The slope value (m) from the regression equation was then divided by 4π (m/4π) to calculate the depth of each zone. The results indicate that the regional zone has an approximate depth of 875,11 meters, the local zone is located at a depth of 278,78 meters, and the noise zone corresponds to a depth of 102,46 meters. This analysis provides a conceptual understanding of the vertical distribution of subsurface anomalies based on the spectral response of gravity data in the Batu Jomba area. A similar study by [33] reported that the spectral analysis of the Great Sumatran Fault in the Dikit Segment yielded a regional depth of 1.051,8 m and a local depth of 196,54 m.

4.4. Euler deconvolution

After performing residual anomaly separation, the Euler deconvolution process can be applied to determine the distribution of anomaly source depths, whether faults, basins, or reservoirs. Prior to conducting the analysis, parameters such as the structural index of the gravity anomaly, window size, and grid mode must first be specified. The following table presents the structural index values for gravity field data under different models.

Table 1. Structural Index Values of the Gravity Field in Different Model (Layade, 2025).

Structural Index	Gravity Field
2	point, sphere
1	thin bed fault
0	thin sheet edge, thin sill, thin dyke
-1	thick sheet edge
Not useful	Contact of infinite depth extent

The selection of an appropriate structural index depends on the expected geometry of the subsurface anomaly sources. As summarized in Table 1, a structural index of 2 corresponds to point or spherical sources, representing compact bodies such as isolated intrusions. An index of 1 is associated with thin bed faults, reflecting elongated or planar discontinuities with limited thickness. A structural index of 0 represents thin sheet edges, thin sills, or thin dykes, which are characterized by laterally extensive but vertically constrained geometries. An index of −1 corresponds to thick sheet edges, typically representing broader tabular structures. In contrast, contacts of infinite depth extent are considered not suitable for Euler deconvolution analysis, as they do not satisfy the homogeneity assumptions required by the method.

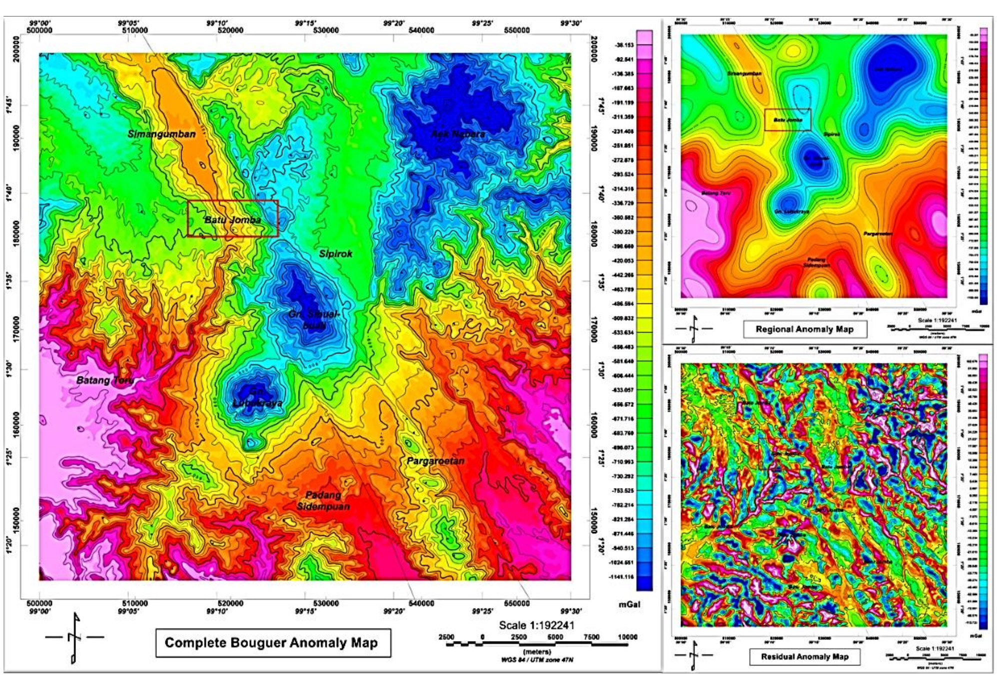

Figure 6. Complete Bouguer anomaly map (left), regional anomaly map (top right), and residual anomaly map (bottom right) of the Batu Jomba landslide-prone road corridor.

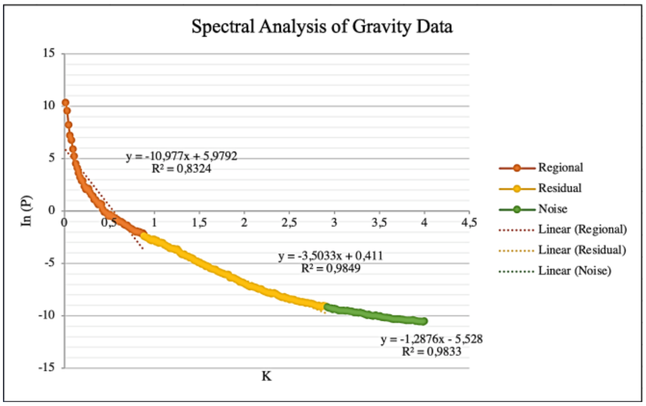

Figure 7. Spectral analysis of gravity field data, categorizing the spectra into three main components: regional, residual (local), and noise.

For fault detection and structural mapping in this study, a structural index of 0 was selected, as faults are generally modeled as thin sheet-like discontinuities in the gravity field. This assumption effectively captures the lateral density contrasts produced by juxtaposed rock units along fault planes, enabling reliable delineation of secondary fault structures within the Batu Jomba area [34].

the Batu Jomba area, clustered Euler solutions in adjacent zones indicate significant subsurface structural related to the area.

The results of Euler deconvolution mapping in the Batu Jomba area, Sipirok District, reveal the distribution of anomaly boundary points representing subsurface structures with varying depths. No depth solutions were directly detected within the Batu Jomba area. Clustered Euler solutions in adjacent zones nearby area indicate significant subsurface structures with depths ranging from 193 to 590 m. The Toru Segment exhibits tectonic activity at depths of 193–590 m while the Angkola Segment at depths of 193–1.082 m. Batu Jomba is located within the Sihapas Formation (Tms2), which is characterized by sandstone. The calculated Bouguer density value is 2,0454 g/cm³. In comparison, the depth of the Lembang Fault, as determined through Euler deconvolution analysis, lies between 820 and 1.096 meters and is predominantly associated with the Cilanang Formation, characterized by limestone with a density ranging from 2,52 to 2,83 g/cm³ [12].

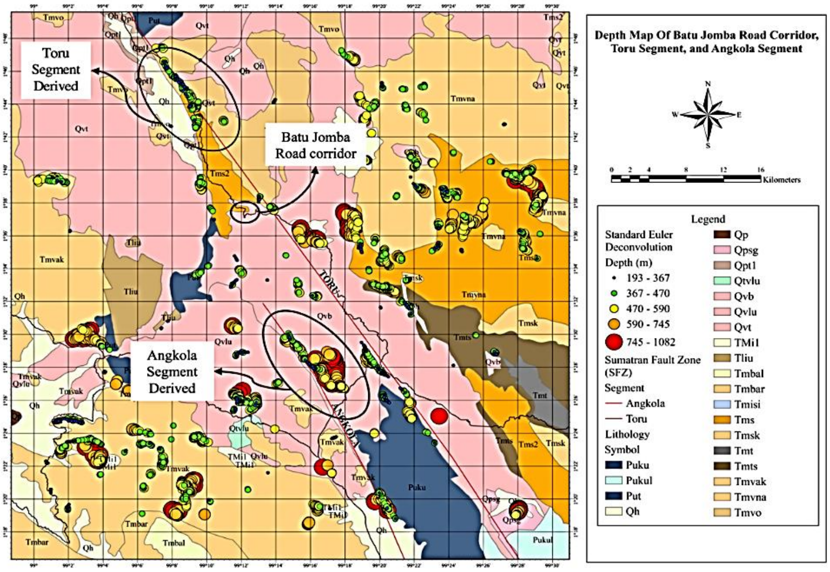

Figure 8. Euler deconvolution depth map of the Batu Jomba road corridor, Toru Segment, and Angkola Segment (appeared in map). While no depth solutions are directly detected along the Batu Jomba area, clustered Euler solutions in adjacent zones indicate significant subsurface structural related to the area.

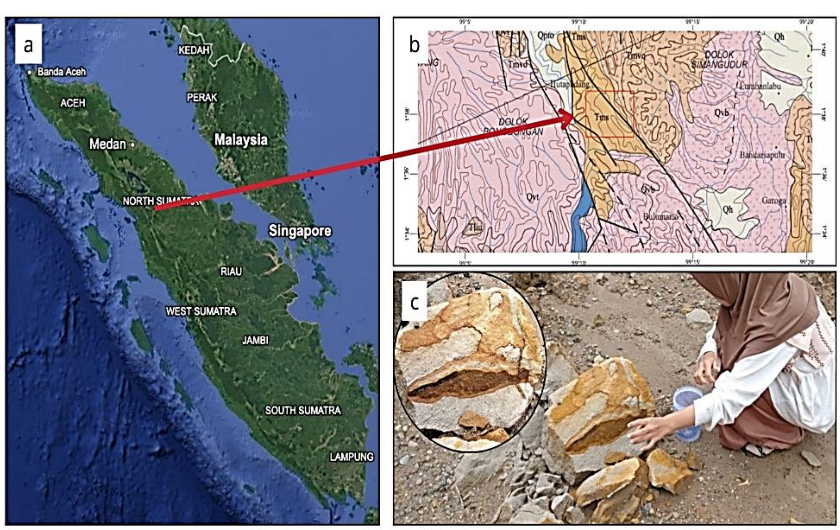

Figure 9. Field observation in Batu Jomba road corridor (a) A satellite map of Sumatra Island, Indonesia (b) Geological sheet of Padang Sidempuan from Ministry of Energy and Mineral Resources (c) A close-up view of the rocks shows layers and textures.

The depth variations indicate significant differences in subsurface geological characteristics, where the Batu Jomba area is dominated by shallow structures, while the Toru and Angkola Segments represent major and deeper fault zones. This suggests the presence of deep subsurface structures overlain by clusters of smaller, shallower structures. Geologically, this zone represents a stepped fault system, functioning as the main conduit for deformation or fluid migration, with secondary fractures forming above it as a response to deeper tectonic stresses [35]. The accumulation of anomalies at shallow depths above deeper anomalies reflects density contrasts and layered sources which may result from rock stratification, subsurface intrusions, or interactions between older and younger faults [36]. This visualization provides a more comprehensive depiction of the subsurface morphology in the Batu Jomba area and reinforces the interpretation derived from the previous two-dimensional analysis.

Field analysis was conducted in Batu Jomba, Luat Lombang Village, Sipirok District, South Tapanuli Regency. Figure 9 illustrates the study area, which is in Figure 9a, the research location map on Sumatra Island shows the trace of the Sumatran Fault stretching from the northern to the southern part of the island. Figure 9b presents the regional geological map of the Padang Sidempuan Sheet, where the symbol *Tms* indicates the Batu Jomba area, representing the Sihapas Formation characterized by sandstone lithology. The discovery of sandstone blocks from landslide debris in Batu Jomba, as shown in Figure 9c, reinforces the statement that this area is dominated by sedimentary rocks with relatively low density, consistent with the measured average density of 2,0454 g/cm³. Based on observations of local geological data, the dominant rock in this area is sandstone**,** which exhibits relatively high porosity, permeability, and density. These characteristics make it susceptible to weathering and mass movement when exposed to water.

5. Conclusion

Based on the research conducted, several conclusions can be drawn as follows:

• The Batu Jomba area is characterized by a low Bouguer density of 2.0454 g/cm³, consistent with the Sihapas Formation dominated by weak sandstone lithology. This low-density sedimentary rock exhibits high porosity and permeability, making it highly susceptible to weathering and mass movement when exposed to water. Field observations confirming the presence of sandstone boulders within the landslide debris support this interpretation and indicate that weak lithology is a primary triggering factor for slope instability in this area.

• Euler deconvolution analysis reveals no direct structural expression beneath the Batu Jomba landslide body itself. However, clustered depth solutions in adjacent areas (193–590 m) indicate the presence of a localized secondary fault structure distinct from the main Toru Segment. Regional depth patterns show that the Toru Segment exhibits tectonic activity at depths of 193–590 m, while the Angkola Segment displays deeper structural features at 193–1,082 m. The shallower depth characteristics of the Toru Segment and Btu Jomba area compared to the Angkola Segment support previous interpretations of crustal thinning beneath North Sumatra, driven by regional extensional stress at depths of approximately 20 km.

• The spatial distribution and depth variations of Euler solutions suggest a stepped fault system, where the main Toru Segment acts as the primary conduit for tectonic deformation, with secondary fractures and subsidiary faults forming in the shallow subsurface as a response to deeper tectonic stresses. The absence of direct fault expression beneath the Batu Jomba landslide body, combined with the proximity of secondary fault structures, indicates that landslide occurrence in this corridor is controlled primarily by the interaction between weak lithology and nearby fault-related deformation rather than direct displacement along the main Toru Segment.

• Further investigation combining additional geophysical methods (such as seismic reflection, magnetotelluric, or InSAR) with detailed geological mapping and geotechnical analysis would provide a more comprehensive understanding of the subsurface structure and landslide mechanisms in the Batu Jomba area. Long-term monitoring of ground deformation using GPS or InSAR techniques could also help quantify the relationship between fault creep, secondary fault activity, and slope displacement rates.

Acknowledgments

The authors would like to express their sincere gratitude to the Department of Physics, Universitas Islam Negeri Sumatera Utara, for the academic and technical support provided throughout the course of this research. The authors also highly appreciate the availability of GGMplus gravity data from Curtin University, which was essential for the Euler deconvolution analysis in this study.

References

[1]. Li, Y., Zhang, H., Huang, L., Li, H., & Wu, X. (2023). The formation mechanism of landslides in typical fault zones and protective countermeasures: A case study of the Nanpeng River fault zone. Front Earth Sci (Lausanne), 10, 1-11 doi: 10.3389/feart.2022.1092662.

[2]. Wafi, A., Himawan, T. S., Daru, J. S., & Rikal, A. (2023). Analisis struktur bawah permukaan tanah dengan menggunakan metode geolistrik dan sondir. *Prosiding Seminar Nasional dan Pameran Metode dan Teknologi Bidang Konstruksi.*

[3]. Kodoatie, R. J. (2012). Tata ruang air tanah. Yogyakarta: *Penerbit ANDI.*

[4]. Kusumartono, H., & Heston, Y. P. (2010). Kajian sosial ekonomi ruas jalan alternatif Aek Latong (Tarutung-Sipirok). Kajian Sosial Ekonomi Ruas Jalan Alternatif Tarutung.

[5]. Rambe, E. I. (2013). Pendeteksian struktur tanah dan batuan dengan metode geolistrik resistivity konFigureurasi schlumberger di daerah Aek Latong Sipirok Tapanuli Selatan. Unimed Repository.

[6]. Natawidjaja, D. H. (2018). Major bifurcations, slip rates, and a creeping segment of sumatran fault zone in Tarutung-Sarulla-Sipirok-Padangsidempuan, Central Sumatra, Indonesia. Indonesian Journal on Geoscience 5(2): 137–160. https://doi.org/10.17014/IJOG.5.2.137-160.

[7]. Hutasuhut, B. P. (2023). Dampak sosial relokasi jalan Aek Latong," Sinar Tabagsel. https://www.sinartabagsel.web.id/2024/08/dampak-sosial-relokasi-jalan-aeklatong.html

[8]. Sieh, K., & Natawidjaja, D. (2000). Neotectonics of the Sumatran fault, Indonesia. Journal of Geophysical Research 55(B12): 28295–28326. https://doi.org/10.1029/2000jb900120.

[9]. Reynolds, J. M. (2011). An introduction to applied and environmental geophysics. Wiley-Blackwell.

[10]. Kurniadi,Y. (2017). Identifikasi zona sesar menggunakan metode gravity di wilayah Ciater, Subang, Jawa Barat. Bandung: ITB Press.

[11]. Lestari, D. P. (2023). Pemodelan inversi data gaya berat dan penerapan penggunaan metode euler deconvolution untuk mendelineasi struktur regional segmen Sesar Cepu. Yogyakarta: UIN Sunan Kalijaga Press.

[12]. Aziz, K. N., Fitrianingtyas, R., Darmawan, D., & Laatifah, L. (2023). Analisis euler deconvolution untuk mengidentifikasi Patahan Lembang berdasarkan data gravitasi. *Jurnal Geofisika* 21(2): 20-26. http://dx/doi.org/10.36435/jgf.v21i2.558.

[13]. Foluronso, I. O., Magaji, Y., Ajadi, J., & Umar, I. (2023). Application of euler and werner deconvolution techniques in

delineating tin deposit in Okeso area, Southwestern, Nigeria. Proceedings of the Nigerian Society of Physical Sciences: 96. https://doi.org/ 10.61298/pnspsc.2024.1.96.

[14]. Chukwu, C., Betts, P., Moore, D., Munukutia, R., Armit, R., McLean, M., & Grose, L. (2024). Unsupervised machine learning and depth clusters of Euler deconvolution of magnetic data: a new approach to imaging geological structures. Exploration Geophysics 55(3): 223–245. https://doi.org/10.1080/08123985.2023.2299475.

[15]. Mono, J. A., Bouba, A., & Nguiya, S. (2024). Edge detection and depth estimation using a tilt angle and euler deconvolution from combined terrestrial and grace gravity data of the Adamawa Plateau Region (North-Cameroon). Journal Of Applied Physics (IOSR-JAP) 16(4): 11–19. https://doi.org/10.9790/4861-1604011119.

[16]. Ghosh, G. K. (2022). Delineation of major subsurface structural features and source depth locations using 3-D Euler deconvolution of gravity data at north-eastern part of India. Acta Geophysica 70(5): 2033–2044. https://doi.org/10.1007/s11600-022-00829-0.

[17]. Muksin, U., Bauer, K., & Haberland, C. (2013). Seismic Vp and Vp/Vs structure of the geothermal area around tarutung (north sumatra, indonesia) derived from local earthquake tomography. Journal of Volcanology and Geothermal Research 260, 27–42. https://doi.org/10.1016/j.jvolgeores.2013.04.012.

[18]. Hickman, R. G., Dobson, P. F., Gerven, M., Sagala, B. D., & Gunderson, R. P. (2004). Tectonic and stratigraphic evolution of the sarulla graben geothermal area, North Sumatra, Indonesia. Journal of Asian Earth Science 23(3): 435–448. https://doi.org/ 10.1016/S1367-9120(03)00155-X.

[19]. Lai, Y., Chung, S., Ghani, A. A., Murtadha, S., Lee, H., & Chu, M. (2021). Mid-miocene volcanic migration in the Westernmost Sunda Arc induced by India-Eurasia collision. Geology, The Geological Society of America 49(6): 713–717. https://doi.org/10.1130/G48568.1

[20]. Siringoringo, L. P., Sapiie, B., Rudyawan, A., & Sucipta, I. G. B. E. (2024). Origin of high heat flow in the back-arc basins of Sumatra: An opportunity for geothermal energy development. Energy Geoscience 5(2024): 1-16. https://doi.org/10.1016/j.engeos.2024.100289

[21]. Lismawaty., Pinem, D. E., & Lubis, G. (2022). Analisa batupasir formasi sihapas sebagai batuan pembawa hidrokarbon (reservoar rock) daerah Gunung Tua-Sumatera Utara. Jurnal Sains dan Teknologi 17(1): 1-6. https://doi.org/10.59637/jsti.v17i1.137

[22]. Barber, A. J., & Crow, M. J. (2005). Chaper 13: Structure and structural history. Geological Society Publications 31: 175-233. https://doi.org/10.1144/GSL.MEM.2005.031.01.13

[23]. Jayatri, A, U., Multi, W., & Hayatuzzahra, S. (2023). Identifikasi keberadaan sesar menggunakan metode gravitasi dan analisis second vertical derivative (svd) di Bagian Selatan Kabupaten Sumbawa. Jurnal Tambora 7(2): 53-37. https://doi.org/10.36761/jt.v7i2.2954

[24]. Daoud, A. M. A., Shebl, A., Abdelkader, M. M., Mohieldain, A. A., Csamer, A., Satti, A. M. N., & Rozsa, P. (2025). Remote sensing and gravity investigations for barite detection in Neoproterozoic rocks in the Ariab area, Red Sea Hills, Sudan. Remote Sensing Application 37(2025): 1-27. https://doi.org/10.1016/j.rsase.2024.101416

[25]. Sudrajad, B. (2023). Analisis deskriptif perbandingan data sekunder gravitasi GGMplus terhadap data gravitasi lapangan panas bumi Gunung Lawu dan data gravitasi stasiun referensi (gravity base station) di Pulau Papua. Jurnal Fisika Papua 2(1): 25–34. https://doi.org/10.31957/jfp.v2i1.22

[26]. A. S. Visca., M. Syafwan., & A. R. Putri. (2019). Interpolasi splin kubik terapit. *Jurnal Matematika,* 7(2), 141-148.

[27]. Rhamadani, D. A. & Saputra, E. E. D. (2023). Analisa model machine learning dalam memprediksi laju produksi sumur migas 15/9-F-14H. Jurnal Ilmu Fisika dan Pembelajarannya (JIFP) 6(2): 23-30. https://doi.org/10.19109/jifp.v6i2.13958

[28]. Telford, W. M., Geldart, L. P., & Sheriff, R. E. (1990). Applied geophysics (Vol.1). Cambridge university press.

[29]. Febridon, M. N., Mulyatno, B. S., & Wijaksono, E. (2020). Analisis sifat fisis pada reservoar batupasir menggunakan metode seismik inversi impedansi akustik (ai) dan multiatribut pada Lapangan 'Mnf' Cekungan Bonaparte. JGE (Jurnal Geofisika Eksplorasi) 4(2): 118–128. https://doi.org/10.23960/jge.v4i2.11

[30]. W. G. A. Kadir, S. Sukmono, M. T. Zen, L. Hendrajaya, and D. Santoso, "Gravity Evidence for The Thinning of The Crust Around The North Sumatera Area," in *Indonesian Petroleum Association*, The AAPG/Datapages Combined Publications Database, 1996.

[31]. Hidayat, S., Lubis, L. H., & Parera, A. F. T. (2023). Analisis potensi geothermal Gunung Sibualbuali menggunakan metode gravity. Gravitasi 6(2): 14-19. https://doi.org/10.33059/gravitasi.jpfs.v6i02.8542

[32]. Spector, A., Grant, F.S. (1970). Statistical models for interpreting aeromagnetic data. Geophysics 35 (2), 293–302. https://doi.org/10.1190/1.1440092

[33]. Layade, G. O., Bamidele, E. O., Makinde, V., Bada, B. S., & Edunjobi, H. O. (2025). Qualitative and quantitative interpretation of high-resolution gravity data of Ewekoro, Southwest Nigeria using source parameter imaging and Euler deconvolution techniques. Iranian Journal of Geophysics 18(6): 1–16. https://doi.org/ 10.30499/IJG.2023.398619.1533

[34]. Zaenudin, A., Karyanto., Kurniasih, A., & Wiboow, R. C. (2021). Analisis struktur patahan daerah Suoh menggunakan metode gaya berat dan penentuan kerapatan patahan. POSITRON 11(2): 95-103. https://doi.org/10.26418/positron.v11i2.48461

[35]. Yanis, M., Simanjutak, A. V. H., Abdullah, F., Marwan., & Ghani, A. A. (2023). Application of seismicity and gravity observation-based filtering model for mapping a fault structure in Weh Island, Indonesia. Iraqi Geological Journal 56(2): 260–274. https://doi.org/10.46717/igj.56.2A.20ms-2023-7-29